Earth ArXiv

Erosion-initiated stromatolite formation in a recent hypersaline sabkha setting (Abu Dhabi, United Arab Emirates)

Andreas Paul[1,*], Stephen W. Lokier[1], Wesley M. Court[1], Cees van der Land[2], Luiza L. Andrade[2], Kirsten E. Dutton[2], Angela Sherry[2], and Ian M. Head[2]

[1]Department of Geosciences, The Petroleum Institute of Khalifa University of Science and Technology, P.O. Box 2533, Abu Dhabi, United Arab Emirates
[2]School of Natural and Environmental Sciences, Newcastle University, Newcastle upon Tyne, NE1 7RU, United Kingdom
[*]Corresponding author: apaul.geol@posteo.de

Please carefully note that this article has been submitted for publication and will appear in a revised form in SEDIMENTOLOGY. Subsequent versions of this manuscript may have significantly different or even contradictory content.

Abstract

Laminated microbial mats and microbialites are documented from a variety of coastal marine environments. These features form through: a) the combination of trapping and binding of allochthonous grains, and b) microbially-mediated or controlled precipitation of a variety of minerals, including high-magnesium calcite and dolomite. Intertidal pools and associated microbial features have been previously documented from the coastal sabkha of Abu Dhabi, but have not been studied in detail. This study therefore aims to provide the first detailed descriptions of thrombolite and stromatolite structures in the coastal sabkha complex of Abu Dhabi. These detailed descriptions will be utilised to develop a new model for their formation, and to consider the implications for the interpretation of similar features from the depositional record. It is proposed here that the development of intertidal pools within the laminated microbial mat zone is the result of localised erosion as a result of storm surges and tides. The formation of erosional scours, which continued to develop into the pools observed today, led to a switch in microbial communities from filamentous cyanobacterial mats into coccoid cyanobacterial mats as a result of reduced environmental stress under conditions of permanent flooding. In addition, the continuous circulation of seawater initiated the abiotic lithification of submerged microbial mat and carbonate rudstone by acicular aragonite cements. Simultaneously, (proto-)dolomite was formed in the stromatolites between individual laminae that were enclosed by a bacterial extra-polymeric substance. These structures therefore developed through the combined effects of erosion, abiotic early lithification and microbially-mediated processes, and may actively respond to changes in sea level. The thrombolites and stromatolites therefore represent a link between unlithified laminated microbial mats and domal stromatolites. This model of stromatolite formation has strong implications for the interpretation of similar fossil structures observed in ancient stratigraphic sequences.

1   Introduction

Stromatolites are laminated benthic microbial deposits (Riding, 1999) that form through lithification processes mediated or controlled by microbial communities of archaea, bacteria and/or diatoms (Dupraz et al., 2011). The term stromatolite, Greek for "layered rock", was first introduced by Kalkowsky (1908). Modern stromatolites are well documented from a variety of coastal marine settings, particularly Highborne Cay on the Bahamas (Andres and Reid, 2006; Stolz et al., 2009; Bowlin et al., 2012) and Shark Bay in Western Australia (Logan, 1961; Reid et al., 2003; Jahnert and Collins, 2013). Microbial mat and stromatolite deposits are also common in a variety of other coastal marine settings, including Lagoa Vermelha in Brazil (Vasconcelos et al., 2006), Cayo Coco lagoon on Cuba (Bouton et al., 2016), the Dohat Faishakh sabkha in Qatar (Brauchli et al., 2016), the Caicos Platform in the western Atlantic Ocean (Trembath-Reichert et al.,

1

47 2016) and the sabkha complex of Abu Dhabi in the United Arab Emirates (Evans, 1966; Kendall and Skipwith,
48 1968; Court et al., 2017). Thrombolitic, hemispheroid microbial mat deposits and stromatolite-like features
49 were previously briefly mentioned from the coastal sabkha of Abu Dhabi (Kendall and Skipwith, 1968), yet,
50 to date, no detailed description and interpretation of these features has been undertaken.

51 This study aims to provide the first detailed descriptions of the thrombolite and stromatolite structures in
52 the coastal sabkha complex of Abu Dhabi. These detailed descriptions will be utilised to develop a new
53 model for their formation, and to consider the implications for the interpretation of similar features from
54 the depositional record.

2 Study area

56 The study area is located in the southeastern Arabian/Persian Gulf, herein referred to as the Gulf, ap-
57 proximately 50 km to the southwest of Abu Dhabi City (Fig. 1 A, B). The Gulf is classified as a shallow,
58 Mediterranean-type sea, indicating that water circulation is induced mainly by seasonal salinity and tem-
59 perature differences (Dietrich, 1980). Water depth in the Gulf is 35 m on average, reaching 100 m in the
60 Strait of Hormuz (Purser and Seibold, 1973). The Gulf exhibits a micro-tidal regime with a tidal range of 1.5
61 m in open marine areas and less than 1.0 m in the lagoons (Evans, 1970). The southern coastline of the Gulf
62 experiences annual temperature variations between 7 °C during winter months and 50 °C during summer
63 months (Lokier, 2012). Annual average rainfall reaches a maximum of 72 mm, with most of this precipita-
64 tion occurring during storm surges in winter months from December to March (Raafat, 2007). Evaporation
65 (2750 mm per year) far exceeds rainfall (Bottomley, 1996).

66 The southeastern part of the Gulf is a northward-sloping carbonate ramp depositional system s.l. Wilson
67 (1974). Environmental conditions on this carbonate ramp initially facilitated the deposition of mixed silici-
68 clastic-carbonate sands as a result of the transgression that followed the last glacial maximum (Evans et al.,
69 1969; Lambeck, 1996; Lokier and Steuber, 2008). The initial formation of a vast microbial mat belt and
70 associated evaporites commenced during the stillstand with a subsequent decrease in the rate of relative
71 Holocene sea level rise between 7,100 - 6,890 cal yrs BP (Lokier et al., 2015). This was followed by the
72 retrogradation of surficial microbial and evaporite facies belts as a result of further relative sea-level rise,
73 a highstand during the Atlantic stage in the Middle Holocene, and subsequent progradation during the
74 middle to late Holocene fall in relative sea level (Lokier and Steuber, 2008; Lokier et al., 2015).

75 From seaward to landward, surface facies of the modern sabkha (Fig. 1 C) consists of peloidal carbonate
76 sands in the lower and middle intertidal zone (lagoon), a coast-parallel microbial mat belt in the upper
77 intertidal zone, and evaporite precipitates in the supratidal zone (Evans et al., 1969; Kendall and Skipwith,
78 1969). The spatial occurrence of these facies belts is controlled by the local angle of slope and therefore
79 depends on the duration of daily flooding by the tides (Court et al., 2017) . The microbial mat belt varies in
80 width between 150 to 800 m and is classified based on surface morphologies that result from the duration
81 of daily flooding. From seaward to landward, these zones are: cinder, polygonal, crinkle and flat zone
82 (Kendall and Skipwith, 1968).

3 Methodology

84 Satellite imagery provided by Google Earth Pro was used to identify areas in the intertidal zone where
85 channels and pools were present. A field reconnaissance campaign in January 2016 identified an area con-
86 taining an ephemeral ponds network, tidal channels and the intertidal pool that is the focus of this study.
87 The morphology of the pool was mapped using a Garmin GPSmap 78 device; the data was subsequently
88 imported and processed in Quantum GIS 2.18 (Quantum GIS Development Team, 2009). Microbial fea-
89 tures, stromatolite-like features, thrombolites and other sedimentary and/or biological characteristics of
90 the pool were comprehensively documented. Subsequent monitoring and sampling visits were made from
91 January 2016 and May 2017. Any visible changes to the morphology of the pool and individual features
92 were documented during these visits, including colour, size and shape thrombolites, sediments within the
93 pool, of the stromatolites and of the surrounding microbial mat. Three specimens of stromatolite from the
94 margin and one specimen of thrombolite from the pool centre were manually recovered and subsequently
95 stored in seawater in plastic containers.

A GP1 compact weather station (Delta-T Devices) was used to measure atmospheric data between April 2016 and July 2017. The station was installed 3 km landwards from the studied pool, at 1.20 m above ground surface (Fig. 1 C). The station continuously measured air temperature, air humidity, wind direction, wind speed, and precipitation. Due to a battery failure, no data is available for February and March 2017. Barometric pressure and additional temperature data was measured at 30 minute intervals between February 2016 and June 2017 with a Baro-Diver barometric logger (Van Essen Instruments). Barometric pressure was used to compensate the water level logger data (see below). The lateral distance between GP1 weather station and barometric logger was approximately 2 km (see Fig. 1 C). Data analysis and visualisation were conducted in the statistical computing language R (R Core Team, 2017), in the programming language Python version 2.7.10 (Van Rossum, 1995) and in PAST version 3.15 (Hammer et al., 2001).

The physico-chemical characteristics of the water in the studied pool were measured using an Ultrameter II 6PFC device (Myron L Company), which provided point data on temperature, conductivity, total dissolved solids (TDS), oxidation-reduction potential (ORP), resistivity and pH. Due to the very high amounts of dissolved solids in the water, resistivity measurements with the Ultrameter II were off-scale at all times and, thus, were not used for further interpretations. Salinity was measured using a Brix-type refractometer with automatic temperature compensation. Water level was monitored from February to October 2016 using a CTD-diver water level logger installed 5 cm above the pool base within a sill that is open on two sides (Van Essen Instruments). Water level was recorded as pressure in mbar, with a barometric conversion applied by subtracting barometric pressure from the water level pressure, under the assumption that 1 mbar = 1 cm of H_2O.

The stromatolite features were investigated at the micro-scale using a Quanta 200 (FEI) scanning electron microscope (SEM), located at The Petroleum Institute of Khalifa University of Science & Technology. One hand specimen was selected from which representative sections were broken off, cleaned with compressed air, mounted on metal stubs, and coated with a palladium/gold mixture. The energy-dispersive X-ray spectroscopy mode (EDX) of the SEM was used to semi-quantitatively characterise element compositions of specific features such as unknown mineral phases.

Standard-sized petrographic thin sections were prepared from three stromatolite specimens including the specimen that was investigated in the SEM. The pieces were cut using a diamond rock saw and subsequently left to dry in the laboratory for 24 hours. Each sample was then impregnated with blue resin in a vacuum chamber in order to enhance the visibility of pore space under the optical microscope.

4 Results

4.1 Environmental Data

Air temperatures recorded by the GP1 weather station ranged between 8.4 °C and 48.9 °C; air temperatures recorded by the barometric logger ranged between 8.9 °C and 53.7 °C (Fig. 2 A). The highest temperatures were recorded during July and August, while the lowest temperatures were recorded during February. Total precipitation during the measurement period amounted to 7.6 mm, mainly resulting from torrential rainfall events in January and February 2017 (Fig. 2 A). March 2017 experienced heavy rainfall, but, as previously mentioned, this data was not recorded by the weather station due to a battery failure. Therefore, the rainfall data represent a minimum value for the measurement interval. The primary wind direction throughout the recording period was from the north-west (Shamal), with secondary winds from the south (Fig. 2 C). Wind directions typically switched twice a day between onshore and offshore due to adiabatic processes. Wind speed varied between 0.3 - 15.4 m/s with a mean of 3.7 m/s (Fig. 2 C, D).

Water temperatures in the pool ranged between 11.7 °C and 46.8 °C during the measurement period (Fig. 2 B). The lowest water temperatures were recorded in February while the highest water temperatures were recorded in August. Salinity ranged between 75.0 ‰ to 93.0 ‰, accompanied by pH values between 7.3 to 8.1. Of the remaining physico-chemical parameters, conductivity values ranged between 100.0 - 118.7 mS/cm, TDS values ranged between 75.0 - 91.26 parts per thousand (ppt), and ORP values ranged from 79 mV to 100 mV.

The tidal regime in the studied pool is semi-diurnal micro-tidal, with a water depth ranging from a minimum of 19 cm up to a maximum of 109 cm (Fig. 2 B).

4.2 Pool morphology and hydrological regime

The data presented here are from an intertidal pool located at the seaward edge of the polygonal zone (star-symbol on Fig. 1 C). These polygons are known to form as a result of organic matter production in a spatially-limited microbial community (Lokier et al., 2017). The studied intertidal pool is horseshoe shaped and open on its seaward and landward sides (Fig. 3 A, B). The seaward opening of the pool corresponds to the landward end of a tidal channel that extends into the lower intertidal and subtidal zones. The landward opening is a narrow lithified sill that forms a connection to an elevated ephemeral pond system (Fig. 4). The pool exhibits a perimeter of 80 m and an area of 250 m^2. The height difference between the floor of the pool and its rim ranges between 20 and 30 cm. The floor of the pool is always submerged beneath seawater, in stark contrast to its location in the mid-intertidal zone.

4.3 Macro-scale sedimentary and biological features

The general stratigraphy at this locality (Fig. 3 C) consists of Pleistocene to early Holocene aeolian siliciclastic sands, overlain by a shallow-marine carbonate hardground of mid-Holocene age (Lokier and Steuber, 2009; Paul and Lokier, 2017), followed by an overlying unconsolidated to lightly-cemented bioclastic rudstone that is further overlain by laminated microbial mat. Though the seaward side of the pool the hardground is locally exposed, the hardground is covered by an organic ooze that measures up to 70 mm thick at the landward side (Fig. 5 A, B).

Accumulations of soft gravel-sized grains are observed throughout the pool. These grains vary in colour and typically accumulate in small troughs and/or in the current-shadow of thrombolite patches and bands. The grains vary in diameter between 5-10 mm and are irregularly shaped (Fig. 6 A). The grains contain sub-mm scale inclusions of bioclastic grains and benthic foraminifera (Fig. 6 B - D).

Clotted microbial (thrombolite) fabrics are distributed within the pool as domal or semi-continuous dm to m-long bands (Fig. 7 A). The structures typically measure between 5-20 cm in width, and exhibit relief above the hardground of between 10-25 cm. The structures are coloured brown to dark brown, and they are characterised by a spongy consistency that likely reflects a dominantly coccoid cyanobacteria composition (*Entophysalis*?). A mm-thick cover of bioclastic grains is present on-top (Fig. 7 B). Marine brown or green algae grow on the outer edges of individual thrombolites marking the absolute minimum water depth within the pool. Internally, the domal structures consist of two intervals (indicated on Fig. 3 C): a 10 cm thick laminated lower stromatolite interval at the base of the thromobolite is attached to the underlying hardground (Fig. 8 B). The upper interval is a true thrombolite and exhibits crude laminations corresponding to differently-coloured microbial communities interlayered with bioclasts (Fig. 8 A).

The margins of the pool exhibit the same vertical facies variations, but are partially-undercut by up to 10 cm (Fig. 9). Moving away from the pool laterally, the coccoid cyanobacterial communities transition within decimetres into a finely-laminated and polygonal filamentous microbial mat (Fig. 10). Elongate scours oriented perpendicular to the shoreline are distributed throughout the polygonal microbial mat zone (Fig. 11). These scours cut through the laminated polygonal microbial mat but do not crosscut individual polygons. They are shallowest at their seaward edge and gradually deepen towards their landward edge. They host a variety of microbial communities that resemble the organic ooze in the pool, with colours ranging from beige to very dark green.

4.4 Micro-facies and structures of lithification features

4.4.1 Petrographic thin sections

The stromatolites of the pool margins consist of microbial extracellular polymeric substance (EPS) draped over apparently acicular aragonite cement and allochthonous grains (Fig. 12 A, B). Bacterial filaments are observed on top of an EPS layer. Where this EPS layer is removed, dolomite precipitates are visible (Fig. 12 C, D). Based on EDX measurements, the crystals contain between 20.71 – 40.37 % Mg, while the surrounding matrix exhibits a significantly lower Mg content of 14% (Fig. 12 C, D). Cyanobacteria are represented by the remainders of bacterial tubes in the matrix surrounding the dolomite crystals (Fig. 12 B, E). At some localities, EPS appears to be draped on-top of the tips of acicular aragonite (Fig. 12 F).

4.4.2 Scanning electron microscopy and EDX

The stromatolites of the pool margin contain lithoclasts, bioclasts and peloidal grains (Fig. 13 A). These grains are enclosed by a dark-coloured microbial layer. Moldic porosity is observed after dissolution of well-rounded peloidal grains (Fig. 13 B). Molds are partially to completely filled by radial acicular aragonite cement. Intergranular pore space is also filled with acicular aragonite cements (Fig. 13 C, D). Microbial and/or organic laminae are discontinuous with a degraded appearance (Fig. 13 E, F).

5 Discussion and Interpretation

5.1 Environmental comparison with other stromatolite provinces

The environmental conditions in the coastal sabkha of Abu Dhabi and in the intertidal pool where observations were made are akin to those of Hamelin Pool in Shark Bay, Western Australia. Commonalities are observed in air and water temperatures, salinity range and in the tidal regime including daily range in water level height (Table 1). Other coastal marine lagoonal stromatolite and/or microbial mat provinces exhibit less extreme overall environmental conditions but share some common characteristics; these include Lagoa Vermelha (Barbiére, 1985; Höhn et al., 1986), Cayo Coco (Bouton et al., 2016) and Highborne Cay of the Bahamas (Andres and Reid, 2006; Bowlin et al., 2012).

5.2 Pool formation and lithification processes

Based upon the observations made during this study, a new model is proposed here for the initiation and evolution of the intertidal pools and their associated microbial features - stromatolites and thrombolites (Fig. 14).

The initial phase of formation of the intertidal pools in the coastal sabkha of Abu Dhabi is the development of erosive scours within the polygonal microbial mat zone (Fig. 14 A to B). These scours form during storm events, spring tides or perigean tides. The removal of the protective layer of trapping and binding microbial mat exposes the underlying unlithified sediments to erosion. Over time, the unlithified sediment is removed and the scours are eroded down to the level of the basal hardground.

The margins of the newly formed pool are susceptible to continued erosion, leading to the lateral extension of the pool (Fig. 14 C, D). In contrast, the areas of sediment that are not eroded are lithified by aragonite cements, possibly as a result of continuous circulation by seawater oversaturated with respect to Ca^{2+} and Mg^{2+} and resulting marine lithification in the Gulf (Shinn, 1969; Wood and Sanford, 2002; Paul and Lokier, 2017). This lithification occurs initially through the dissolution of bioclastic, ooidal or peloidal grains that are trapped between laminated microbial mat layers. The moldic pores that remain after dissolution, as well as intergranular pore spaces, are subsequently filled by acicular aragonite cements. Microbial mediation in the precipitation of this aragonite cement may play a significant role (Reid et al., 2003).

The permanent flooding of the pool is the result of a terracing effect analogous to the flow of water on travertine terraces (Fig. 15; see e.g. Özkul et al., 2014). This leads to an intriguing phenomenon: before the pool is emptied as a result of a low tide, it is already being refilled by the subsequent incoming tide (Fig. 15).

The permanent flooding of the pool results in constant inundation of the microbial mat by seawater, resulting in a switch in microbial communities from filamentous cyanobacteria (that dominated the microbial mats before scour development) to coccoid cyanobacteria (Fig. 14 B to C). Similar relationships between microbial communities and the period of inundation have been documented in Hamelin Pool of Shark Bay, Western Australia, where filamentous cyanobacteria dominate near-shore areas but disappear in areas were inundation times are longer (Suosaari et al., 2016). The coccoid cyanobacterial mats form the observed thrombolite domes and semi-continuous bands observed in the pool. A switch from filamentous microbial communities into coccoid microbial communities has previously been documented to facilitate the precipitation of acicular aragonite (Reid et al., 2000) and explains the large amounts of acicular aragonite observed in the stromatolites. This implies that the lithification of the pool margins is biotically mediated and these features therefore represent "true stromatolites".

The lithification of the sill (Fig. 4) that separates the pool from the ephemeral ponds system is interpreted to result from a combination of microbially-mediated aragonite precipitation and the precipitation of cements as a result of degassing. The partial exposure of the sill at low tide facilitates degassing of the outflowing water, thereby lowering the solubility product of the seawater as it flows over the sill, thereby promoting the abiotic precipitation of cement. This process is similar to the precipitation of carbonates at travertine terraces and tufas (Fig. 15; Gandin and Capezzuoli, 2014; Özkul et al., 2014).

The thrombolites of the coastal sabkha of Abu Dhabi are unlikely to be preserved in the geologic record due to their susceptibility to erosion and degradation of the associated organic matter after burial Kenig et al., 1990; Court et al., 2017. The stromatolites, which form the base of thrombolites as well as parts of the pool margins, possess a significant potential to be preserved in situ in the geologic record after burial. However, the stromatolite structures are of limited lateral extend and are, therefore, likely to be only rarely observed in ancient sequences.

5.3   On the origin of dolomite

Dolomite observed within the stromatolites at the pool margins was enclosed by bacterial EPS and acicular aragonite, with the surrounding matrix also having a high Mg content, though this was not as high as the respective dolomite crystals. This observation supports the microbially-mediated origin of this dolomite in the coastal sabkha of Abu Dhabi as previously proposed (Bontognali et al., 2010). It is possible that, below the EPS layer, a micro-environment develops within which Mg is enriched through microbial processes, a mechanism that has been proposed previously by Bontognali et al. (2010). This proposed mechanism suggests that the enrichment of magnesium will ultimately result in the bacterially-mediated precipitation of dolomite crystals. The data presented here, however, shows no evidence for the direct involvement of bacterial EPS in the growth of the observed dolomite crystals.

5.4   The origin of gravel-sized grains and organic ooze

The grains are likely composed of coccoid cyanobacterial communities akin to those that are observed elsewhere in the pool that form the clotted microbial fabrics of thrombolites. Hence, the softness is the result of their primary composition of bacterial organic matter or EPS. It is likely that these grains are the result of spatially-limited erosion, i.e. they are generated through the break-off of parts or through the complete destruction of thrombolites. Subsequently, they are agitated by low-energy wave and current action, which leads to their shape becoming similar to that of oncoids yet without the concentric laminations (compare to Gerdes et al., 1994). These oncoids-like grains may subsequently be preserved in the geologic record as trace fossils if the amount of bioclasts that were incorporated into the bacterial EPS matrix during growth was high. Fossil microbial grains may thus be indicative of a low-energy coastal-marine depositional environment within which clotted microbial fabrics existed.

6   Conclusions

Intertidal pools and associated microbial mats, thrombolites and stromatolites were observed in the coastal sabkha of Abu Dhabi. It is proposed here that the thrombolites, stromatolites and microbial grains are erosional remnants that originally were part of a surrounding filamentous cyanobacterial mat. They developed through the combined effects of erosion, abiotic early lithification and microbially-mediated processes. These microbial features, therefore, represent a potential link between unlithified microbial mat sheets and domal stromatolites, implying that at least some of the domal stromatolites observed today originate from laminated originally non-lithifying microbial mats.

7   Acknowledgements

bial mats as a modern analogue". The authors declare no conflict of interest related to this study. Our sincere appreciation goes to Sion Kennaway for general laboratory and field support, to Warren Marilag for preparing the petrographic thin sections, and to Prasanth Thiyagarajan for his much-needed assistance with the SEM and EDS analyses. Xin Bixiao and Peng Yuan are thanked for their help during the many long field-days in the sabkha of Abu Dhabi.

This pre-print was prepared with LaTeX in TeXnicCenter, with a modified template made by Overleaf for PaleorXiv, a pre-print archive for Paleontology.

References

Andres, M. S. and Reid, R. P. (2006). Growth morphologies of modern marine stromatolites: A case study from Highborne Cay, Bahamas. *Sedimentary Geology*, 185(3):319–328, DOI: 10.1016/j.sedgeo.2005.12.020.

Barbiére, E. (1985). Condições climaticas dominantes na porção oriental da lagoa de Araruama (RJ) e suas implicações na diversidade do teor de salinidade. *Caderno de Ciências da Terra*, 59:34–35.

Bontognali, T. R. R., Vasconcelos, C., Warthmann, R. J., Bernasconi, S. M., Dupraz, C., Strohmenger, C. J., and McKenzie, J. A. (2010). Dolomite formation within microbial mats in the coastal sabkha of Abu Dhabi (United Arab Emirates). *Sedimentology*, 57(3):824–844, DOI: 10.1111/j.1365-3091.2009.01121.x.

Bottomley, N. (1996). Recent climate of Abu Dhabi. In Osborne, P. E., editor, *Desert Ecology of Abu Dhabi*, pages 36–49. Pisces, Newbury.

Bouton, A., Vennin, E., Pace, A., Bourillot, R., Dupraz, C., Thomazo, C., Brayard, A., Désaubliaux, G., and Visscher, P. T. (2016). External controls on the distribution, fabrics and mineralization of modern microbial mats in a coastal hypersaline lagoon, Cayo Coco (Cuba). *Sedimentology*, 63(4):972–1016, DOI: 10.1111/sed.12246.

Bowlin, E. M., Klaus, J. S., Foster, J. S., Andres, M. S., Custals, L., and Reid, R. P. (2012). Environmental controls on microbial community cycling in modern marine stromatolites. *Sedimentary Geology*, 263-264:45–55, DOI: 10.1016/j.sedgeo.2011.08.002.

Brauchli, M., McKenzie, J. A., Strohmenger, C. J., Sadooni, F., Vasconcelos, C., and Bontognali, T. R. R. (2016). The importance of microbial mats for dolomite formation in the Dohat Faishakh sabkha, Qatar. *Carbonates and Evaporites*, 31(3):339–345, DOI: 10.1007/s13146-015-0275-0.

Court, W. M., Paul, A., and Lokier, S. W. (2017). The preservation potential of environmentally diagnostic sedimentary structures from a coastal sabkha. *Marine Geology*, 386:1–18, DOI: 10.1016/j.margeo.2017.02.003.

Dietrich, G. (1980). *General oceanography: an introduction*. J. Wiley, New York.

Dupraz, C., Reid, R. P., and Visscher, P. T. (2011). Microbialites, Modern. In Reitner, J. and Thiel, V., editors, *Encyclopedia of Geobiology*, pages 617–635. Springer Netherlands, ISBN: 978-1-4020-9211-4 978-1-4020-9212-1.

Evans, G. (1966). The Recent Sedimentary Facies of the Persian Gulf Region. *Philosophical Transactions of the Royal Society A: Mathematical, Physical and Engineering Sciences*, 259(1099):291–298, DOI: 10.1098/rsta.1966.0014.

Evans, G. (1970). Coastal and nearshore sedimentation: a comparison of clastic and carbonate deposition. *Proceedings of the Geological Society of London*, 81(3):493–507, DOI: 10.1016/S0016-7878(70)80010-4.

Evans, G., Schmidt, V., Bush, P., and Nelson, H. (1969). Stratigraphy and geologic history of the sabkha, Abu Dhabi, Persian Gulf. *Sedimentology*, 12(1-2):145–159, DOI: 10.1111/j.1365-3091.1969.tb00167.x.

Gandin, A. and Capezzuoli, E. (2014). Travertine: Distinctive depositional fabrics of carbonates from thermal spring systems. *Sedimentology*, 61:264–290, DOI: 10.1111/sed.12087.

Gerdes, G., Dunajtschik-Piewak, K., Riege, H., Taher, A. G., Krumbein, W. E., and Reineck, H.-E. (1994). Structural diversity of biogenic carbonate particles in microbial mats. *Sedimentology*, 41:1273–1294, DOI: 10.1111/j.1365-3091.1994.tb01453.x.

Hammer, Ø., Harper, D. A. T., and Ryan, P. D. (2001). PAST: Paleontological Statistics Software Package for Education and Data Analysis. *Palaeontologia Electronica*, 4(1):9 pp., http://palaeo-electronica.org/2001_1/past/issue1_01.htm.

Höhn, A., Tobschall, H. J., and Maddock, J. E. L. (1986). Biogeochemistry of a hypersaline lagoon east of Rio de Janeiro, Brazil. *The Science of the Total Environment*, 58(1-2):175–185, DOI: 10.1016/0048-9697(86)90086-0.

Jahnert, R. J. and Collins, L. B. (2013). Controls on microbial activity and tidal flat evolution in Shark Bay, Western Australia. *Sedimentology*, 60(4):1071–1099, DOI: 10.1111/sed.12023.

Kalkowsky, E. (1908). Oolith und Stromatolith im nord-deutschen Buntsandstein. *Zeitschrift der deutschen geologischen Gesellschaft*, 60:68–125.

Kendall, C. and Skipwith, S. P. A. (1969). Holocene Shallow-Water Carbonate and Evaporite Sediments of Khor al Bazam, Abu Dhabi, Southwest Persian Gulf. *AAPG Bulletin*, 53(4):841–869, DOI: 10.1306/5D25C803-16C1-11D7-8645000102C1865D.

Kendall, C. G. S. C. and Skipwith, S. P. A. (1968). Recent algal mats of a Persian Gulf lagoon. *Journal of Sedimentary Petrology*, 38(4):1040–1058, DOI: 10.1306/74D71AF5-2B21-11D7-8648000102C1865D.

Kenig, F., Huc, A. Y., Purser, B. H., and Oudin, J.-L. (1990). Sedimentation, distributions and diagenesis of organic matter in a recent carbonate environment, Abu Dhabi, UAE. *Advances in Organic Geochemistry*, 16(4-6):735–747, DOI: 10.1016/0146-6380(90)90113-E.

Lambeck, K. (1996). Shoreline reconstructions for the Persian Gulf since the last glacial maximum. *Earth and Planetary Science Letters*, 142(1-2):43–57, DOI: 10.1016/0012-821X(96)00069-6.

Logan, B. W. (1961). Cryptozoon and Associate Stromatolites from the Recent, Shark Bay, Western Australia. *The Journal of Geology*, 69(5):517–533, DOI: 10.1086/626769.

Lokier, S. and Steuber, T. (2008). Quantification of Carbonate-Ramp Sedimentation and Progradation Rates for the Late Holocene Abu Dhabi Shoreline. *Journal of Sedimentary Research*, 78(7):423–431, DOI: 10.2110/jsr.2008.049.

Lokier, S. and Steuber, T. (2009). Large-scale intertidal polygonal features of the Abu Dhabi coastline. *Sedimentology*, 56(3):609–621, DOI: 10.1111/j.1365-3091.2008.00988.x.

Lokier, S. W. (2012). Development and evolution of subaerial halite crust morphologies in a coastal sabkha setting. *Journal of Arid Environments*, 79:32–47, DOI: 10.1016/j.jaridenv.2011.11.031.

Lokier, S. W., Andrade, L. L., Court, W. M., Dutton, K. E., Head, I. M., van der Land, C., Paul, A., and Sherry, A. (2017). A new model for the formation of microbial polygons in a coastal sabkha setting. *The Depositional Record*, 3(2):201–208, DOI: 10.1002/dep2.33.

Lokier, S. W., Bateman, M. D., Larkin, N. R., Rye, P., and Stewart, J. R. (2015). Late Quaternary sea-level changes of the Persian Gulf. *Quaternary Research*, 84(1):69–81, DOI: 10.1016/j.yqres.2015.04.007.

Özkul, M., Gökgöz, A., Kele, S., Baykara, M. O., Shen, C.-C., Chang, Y.-W., Kaya, A., Hançer, M., Aratman, C., Akin, T., and Örü, Z. (2014). Sedimentological and geochemical characteristics of a fluvial travertine: A case from the eastern Mediterranean region. *Sedimentology*, 61:291–318, DOI: 10.1111/sed.12095.

Paul, A. and Lokier, S. W. (2017). Holocene marine hardground formation in the Arabian Gulf: Shoreline stabilisation, sea level and early diagenesis in the coastal sabkha of Abu Dhabi. *Sedimentary Geology*, 352:1–13, DOI: 10.1016/j.sedgeo.2017.02.005.

Purser, B. H. and Seibold, E. (1973). The Principal Environmental Factors Influencing Holocene Sedimentation and Diagenesis in the Persian Gulf. In Purser, B., editor, *The Persian Gulf*, pages 1–9. Springer, Berlin Heidelberg, DOI: 10.1007/978-3-642-65545-6_1.

Quantum GIS Development Team (2009). QGIS Geographic Information System. http://qgis.osgeo.org.

R Core Team (2017). R: A Language and Environment for Statistical Computing. https://www.r-project.org/.

Raafat, H. (2007). Climate of Abu Dhabi Emirate, UAE. In Kumar, A., editor, *Physical geography sector paper*, pages 72–89. Environment Agency Abu Dhabi, Abu Dhabi.

382 Reid, R. P., James, N. P., Macintyre, I. G., Dupraz, C. P., and Burne, R. V. (2003). Shark Bay Stromatolites:
383   Microfabrics and reinterpretation of Origins. *Facies*, 49:299–324, DOI: 10.1007/s10347-003-0036-8.

384 Reid, R. P., Visscher, P. T., Decho, A. W., Stolz, J. F., Bebout, B. M., Dupraz, C., Macintyre, I. G., Paerl, H. W.,
385   Pinckney, J. L., Prufert-Bebout, L., Steppe, T. F., and DesMarais, D. J. (2000). The role of microbes in
386   accretion, lamination and early lithification of modern marine stromatolites. *Nature*, 406(6799):989–
387   992, DOI: 10.1038/35023158.

388 Riding, R. (1999). The term stromatolite: towards an essential definition. *Lethaia*, 32(4):321–330, DOI:
389   10.1111/j.1502-3931.1999.tb00550.x.

390 Shinn, E. A. (1969). Submarine lithification of Holocene carbonate sediments in the Persian Gulf. *Sedi-*
391   *mentology*, 12(1-2):109–144, DOI: 10.1111/j.1365-3091.1969.tb00166.x.

392 Stolz, J. F., Reid, R. P., Visscher, P. T., Decho, A. W., Norman, R. S., Aspden, R. J., Bowlin, E. M., Franks, J.,
393   Foster, J. S., Paterson, D. M., Przekop, K. M., Underwood, G. J. C., and Prufert-Bebout, L. (2009). The
394   Microbial Communities of the Modern Marine Stromatolites at Highborne Cay, Bahamas. *Atoll Research*
395   *Bulletin*, 567:1–29, DOI: 10.5479/si.00775630.567.1.

396 Suosaari, E. P., Reid, R. P., Playford, P. E., Foster, J. S., Stolz, J. F., Casaburi, G., Hagan, P. D., Chirayath, V.,
397   Macintyre, I. G., Planavsky, N. J., and Eberli, G. P. (2016). New multi-scale perspectives on the stro-
398   matolites of Shark Bay, Western Australia. *Scientific Reports*, 6:20557, DOI: 10.1038/srep20557.

399 Trembath-Reichert, E., Ward, L. M., Slotznick, S. P., Bachtel, S. L., Kerans, C., Grotzinger, J. P., and Fischer,
400   W. W. (2016). Gene Sequencing-Based Analysis of Microbial-Mat Morphotypes, Caicos Platform, British
401   West Indies. *Journal of Sedimentary Research*, 86(June):629–636, DOI: 10.2110/jsr.2016.40.

402 Van Rossum, G. (1995). Python tutorial. https://www.python.org.

403 Vasconcelos, C., Warthmann, R., McKenzie, J. A., Visscher, P. T., Bittermann, A. G., and van Lith, Y. (2006).
404   Lithifying microbial mats in Lagoa Vermelha, Brazil: Modern Precambrian relics? *Sedimentary Geology*,
405   185(3-4):175–183, DOI: 10.1016/j.sedgeo.2005.12.022.

406 Wilson, J. L. (1974). Characteristics of carbonate-platform margins. *AAPG Bulletin*, 58(5):810–824.

407 Wood, W. W. and Sanford, W. E. (2002). Hydrogeology and solute geochemistry of the coastal-Sabkha
408   aquifer in the emirate of Abu Dhabi. In H.J. Barth and B. Böer, editors, *Sabkha Ecosystems: Volume I:*
409   *The Arabian Peninsula and Adjacent Countries*, pages 173–185. Springer.

Table 1: Environmental data from a variety of coastal marine stromatolite and microbial mat provinces. Sources for the data: Sabkha: this study and studies given in local settings. Hamelin Pool: Water temperatures, salinity, tidal regime and tidal range from Suosaari et al. (2016); air temperatures, mean annual rainfall and wind speed from `http://www.bom.gov.au`; evaporation from Logan (1961). Lagoa Vermelha: Höhn et al. (1986). Cayo Coco: Bouton et al. (2016). Highborne Cay: Bowlin et al. (2012)

Parameter	Location				
	Sabkha	Hamelin Pool	Lagoa Vermelha	Cayo Coco	Highborne Cay
Air temperature (℃)	8.4 – 53.7	9.2 – 36.9	17.0 – 32.0	20.0 – 32.5	-
Water temperature (℃)	11.7 – 46.8	11.0 – 33.0	23.8 – 36.5	28.0 – 30.0	20.3 – 30.3
Salinity (‰)	75.0 – 93.0	15.8 – 88.1	40 – 84	30 – 80	35
Mean annual rainfall (mm)	72.0	210.4	900	1000	-
Annual evaporation (mm)	2750	2032 - 2286	1300	2100 – 2200	-
Tidal range (m)	1.0	1.0	1.0 – 1.7	0.3	1.0
Mean wind speed (m/s)	3.7	2.8	-	3.9	4.18
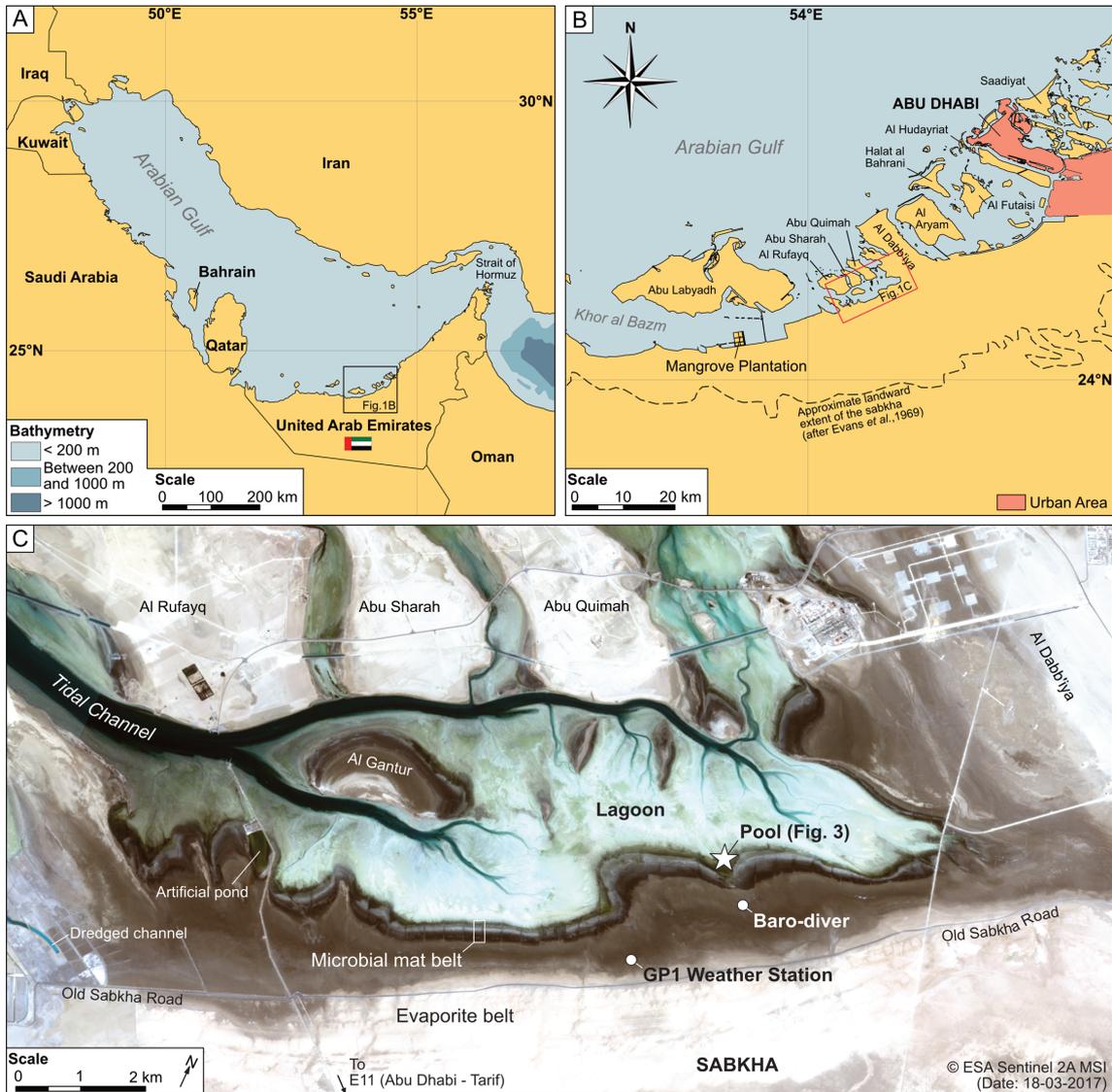
Figure 1: A) Location of the study area in relation to the Arabian Gulf. B) Location of study area in relation to Abu Dhabi. C) The modern coastal sabkha of Abu Dhabi, showing facies belts and anthropogenic changes. The study site is indicated by a white star. Imagery source: ESA Sentinel 2A Multi-spectral Imager (MSI), date 18 March 2017.
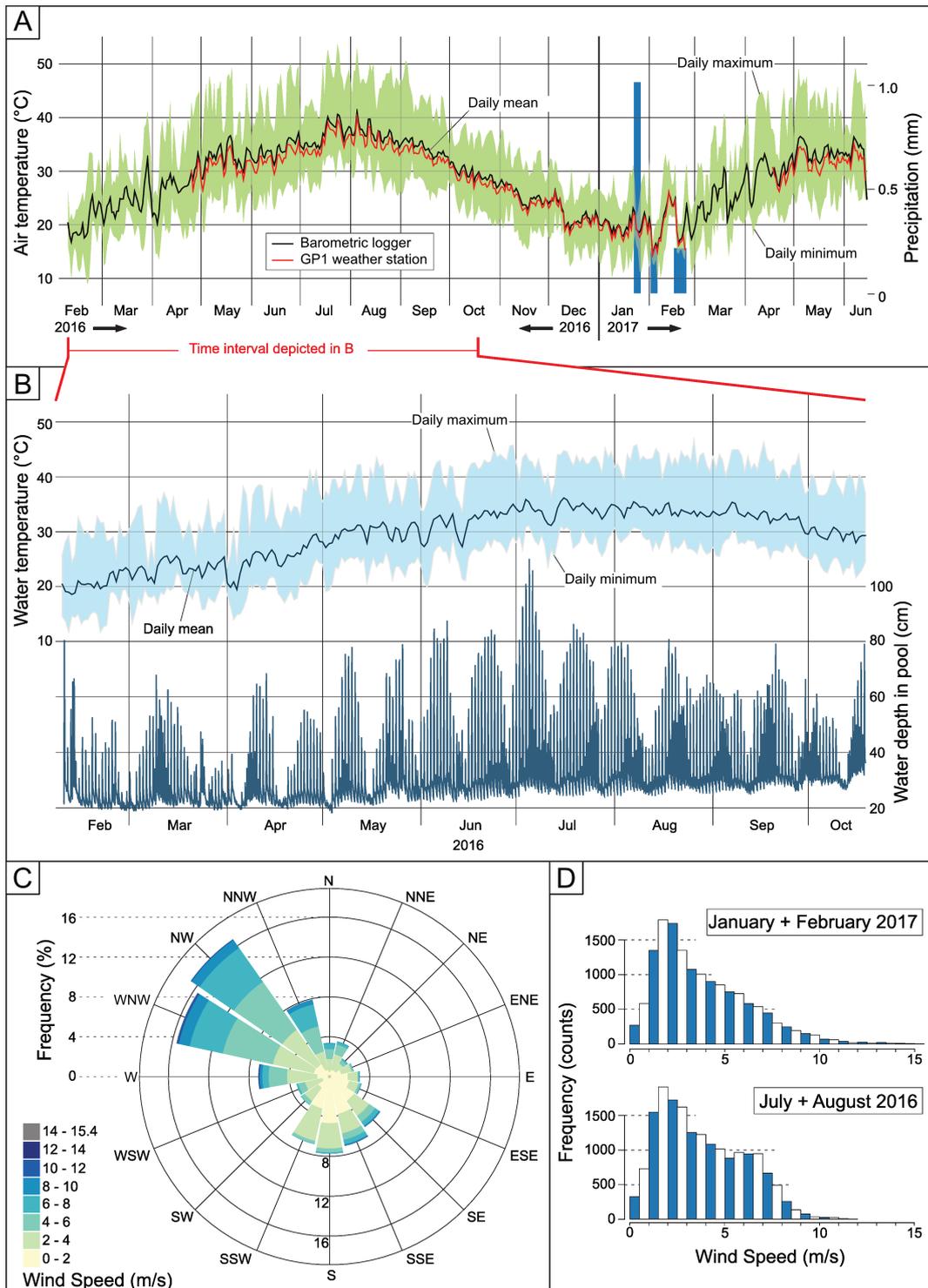
Figure 2: A) Mean daily air temperatures in the coastal sabkha measured between February 2016 and June 2017 using a barometric logger (black) and the GP1 weather station (red). Daily maximum and daily minimum are given in the background. Precipitation in January and February 2017 is also indicated by blue bars. B) Record of water temperatures and water depth in the studied intertidal pool, showing the daily tidal regime as well as long term annual trends in water depth. Note that the pool was never empty despite it being located within the intertidal zone. C) Wind rose showing the dominating wind directions from the WNW - NW and S, and wind speeds. D) Frequency distribution plots of wind speeds for two intervals in January – February 2017 and in July – August 2016. Each vertical bar represents a 0.5 m/s wind speed interval.
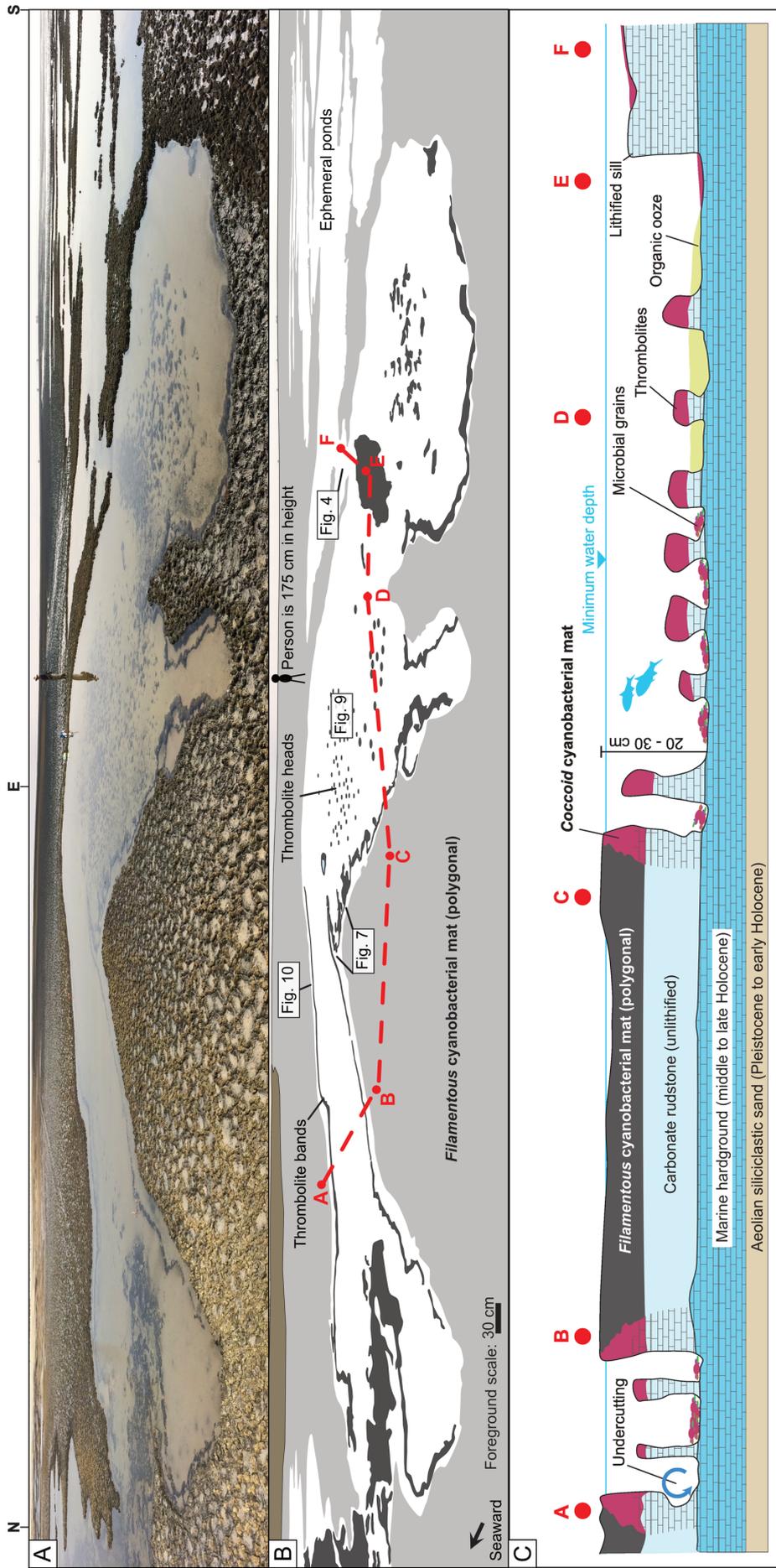
Figure 3: A) Overview photograph of the pool. Note that scale is not uniform from bottom to top due to the way this image was taken; person in background is 175 cm in height. B) Interpretative overview of the features observed in the pool. Seaward direction is on the left. Note the detached bands at the pool margins, and the thrombolites towards the centre of the pool. C) Schematic cross-section through the pool showing the general stratigraphy, lithologies and features described in this study.
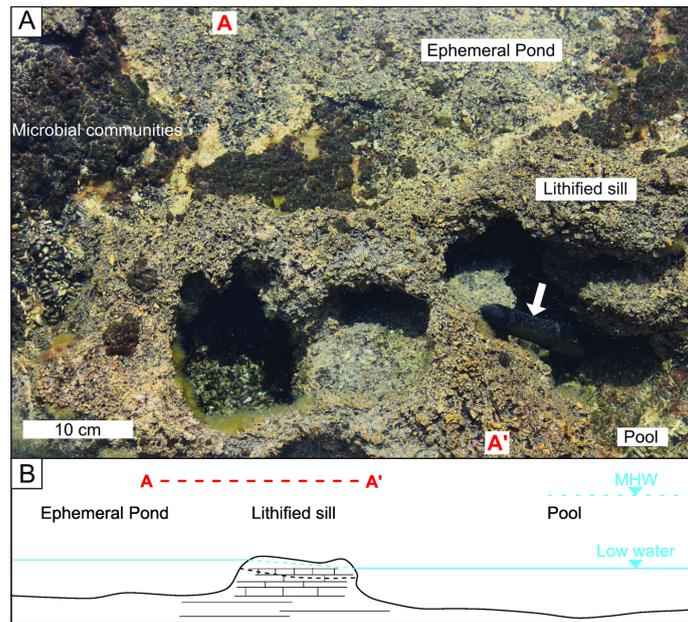
Figure 4: A) Close-up view of the lithified sill. The ephemeral pond system is located at the top, while the pool is towards the bottom (not visible). The lithified sill consists of a carbonate rudstone, and corresponds to the lithified margins in other areas of the pool. The water level logger is indicated by an arrow, the data of which is presented on figure 2. Note the colonisation by cyanobacteria and algae. B) General cross-section with a proposed model with the relationship between ephemeral pond system, lithified sill and the pool.
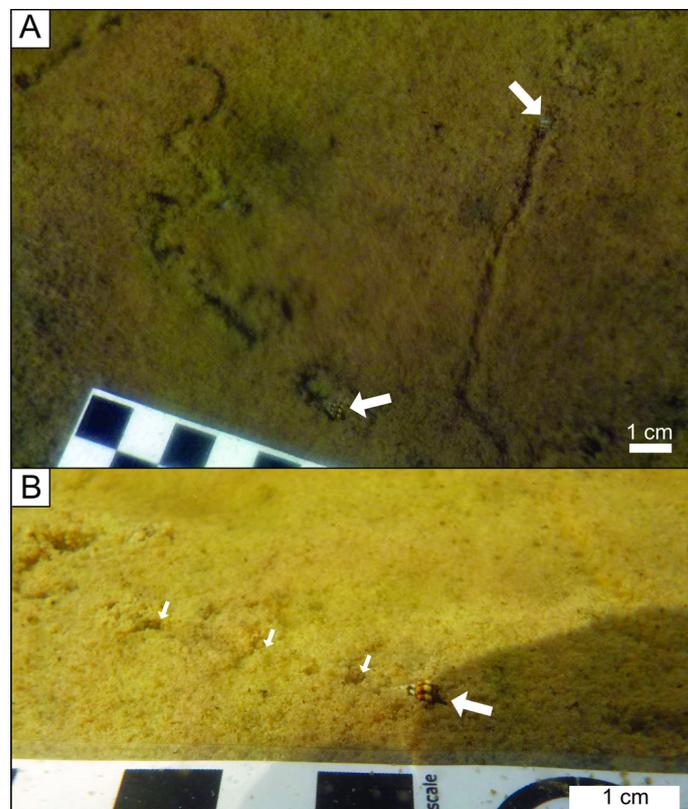
Figure 5: A) Photograph of the organic ooze covering parts of the pool floor. Grazing trails of gastropods are visible with the respective gastropods at the end-points (arrows). B) Close-up view of the ooze and a gastropod (large arrow) and its grazing trail (small arrows).
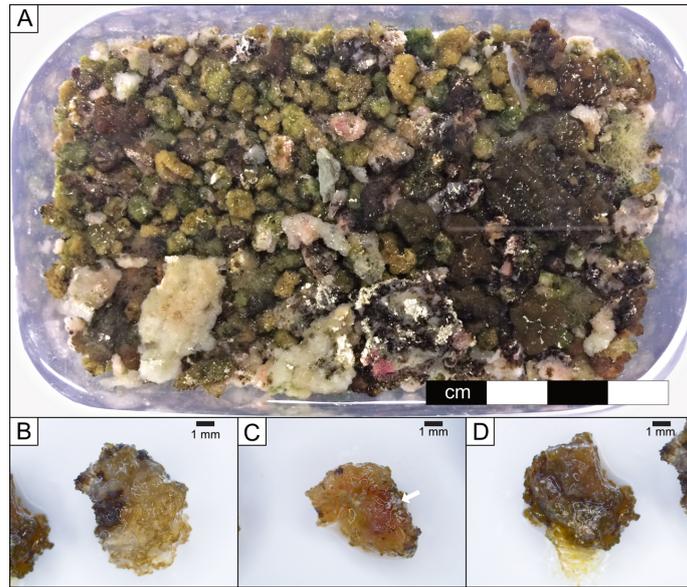
Figure 6: A) Microbial gravel collected from the pool floor. Different colours correspond to different organic pigments. B-D) Close-up views of individual microbial grains showing the EPS and white grains embedded. Grains are bioclasts and benthic foraminifera (arrow).
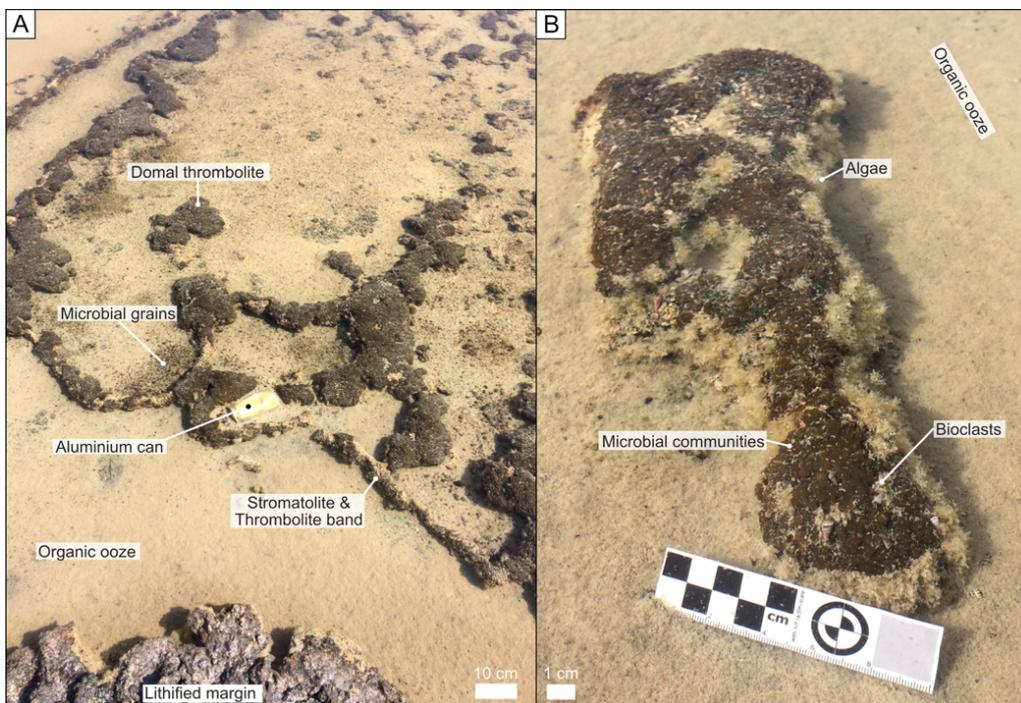

Figure 7: A) Close-up view of different microbial structures including thrombolites and stromatolites. Note the detached rim and the domal and banded thrombolites, surrounded by organic ooze and gravel-sized grains of potentially microbial origin. Note the discarded aluminium can for scale, that is overgrown by microbial communities and is also partially covered by organic ooze. B) Close-up view of an individual thrombolite showing its components: a lithified root (not shown here) covered by organic ooze, brown thrombolite, bioclasts deposited through tidal and/or wind currents, and algae growth. Upper growth boundary of these algae indicates the minimum water depth in the pool, which corresponds to what has been calculated from the water level logger data, approximately 20 cm.
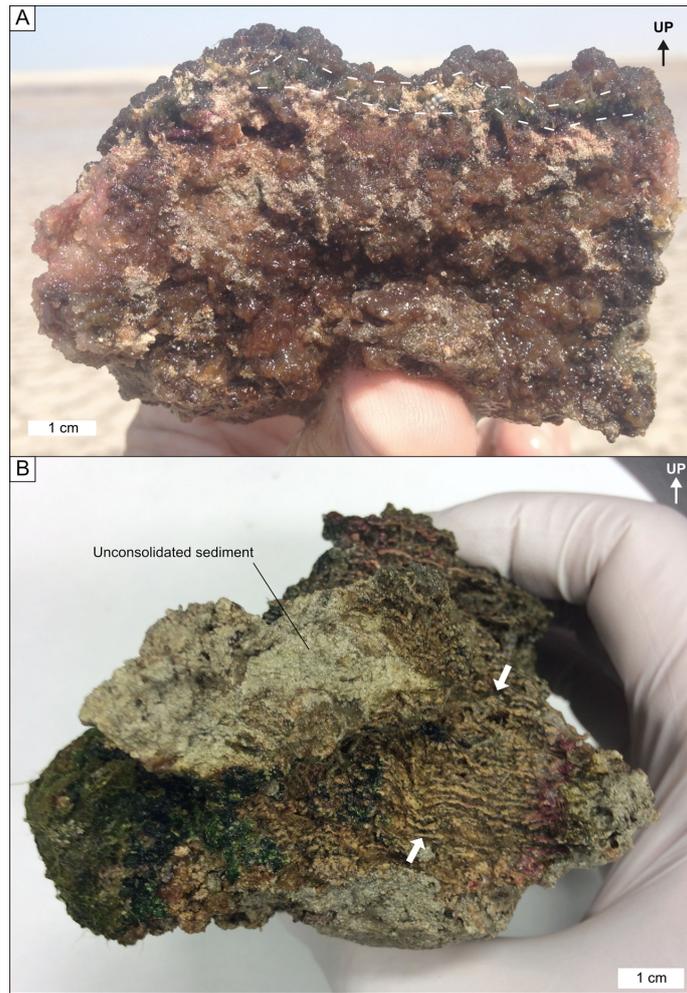
Figure 8: This figure shows vertically the succession from stromatolite to clotted thrombolite fabrics. A) Cross-sectional view of an individual domal thrombolite, showing internal crude radial laminations, based on differences in colour. Bioclasts enclosed by microbial EPS indicate outward growth. Coarse laminae are indicated by broken lines. B) Hand specimen of a stromatolite from the pool margin. Microbial laminations preserved through lithification are clearly visible. Purple and green colours correspond to pigments of living cyanobacterial communities and are unrelated to the primary processes that lead to the development of the stromatolite.
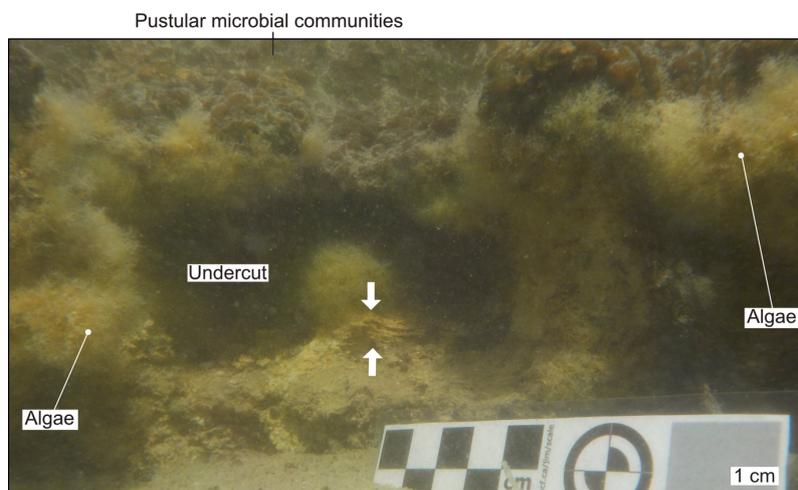
Figure 9: Plane view towards the partially undercut margin at the north-west side of the pool. Note the laminated stromatolites at the centre.
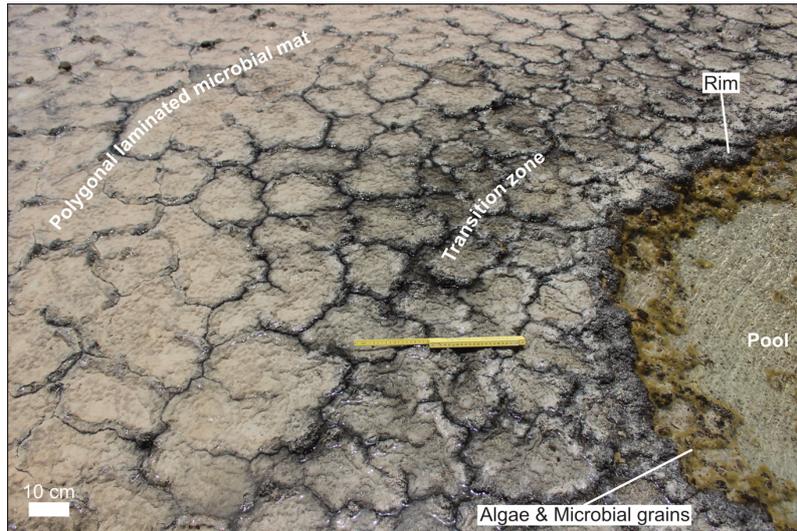
Figure 10: Overview photograph showing the transition from pool via a rim overgrown with algae towards the polygonal microbial mat zone. Note that the polygonal microbial mat in the transition zone appears to be degraded which is likely the result of longer inundation time and an incipient community change from filamentous towards coccoid cyanobacterial communities.

Figure 11: A) An erosive scour observed in the coastal sabkha of Abu Dhabi. B) Schematic cross-section through the scour.
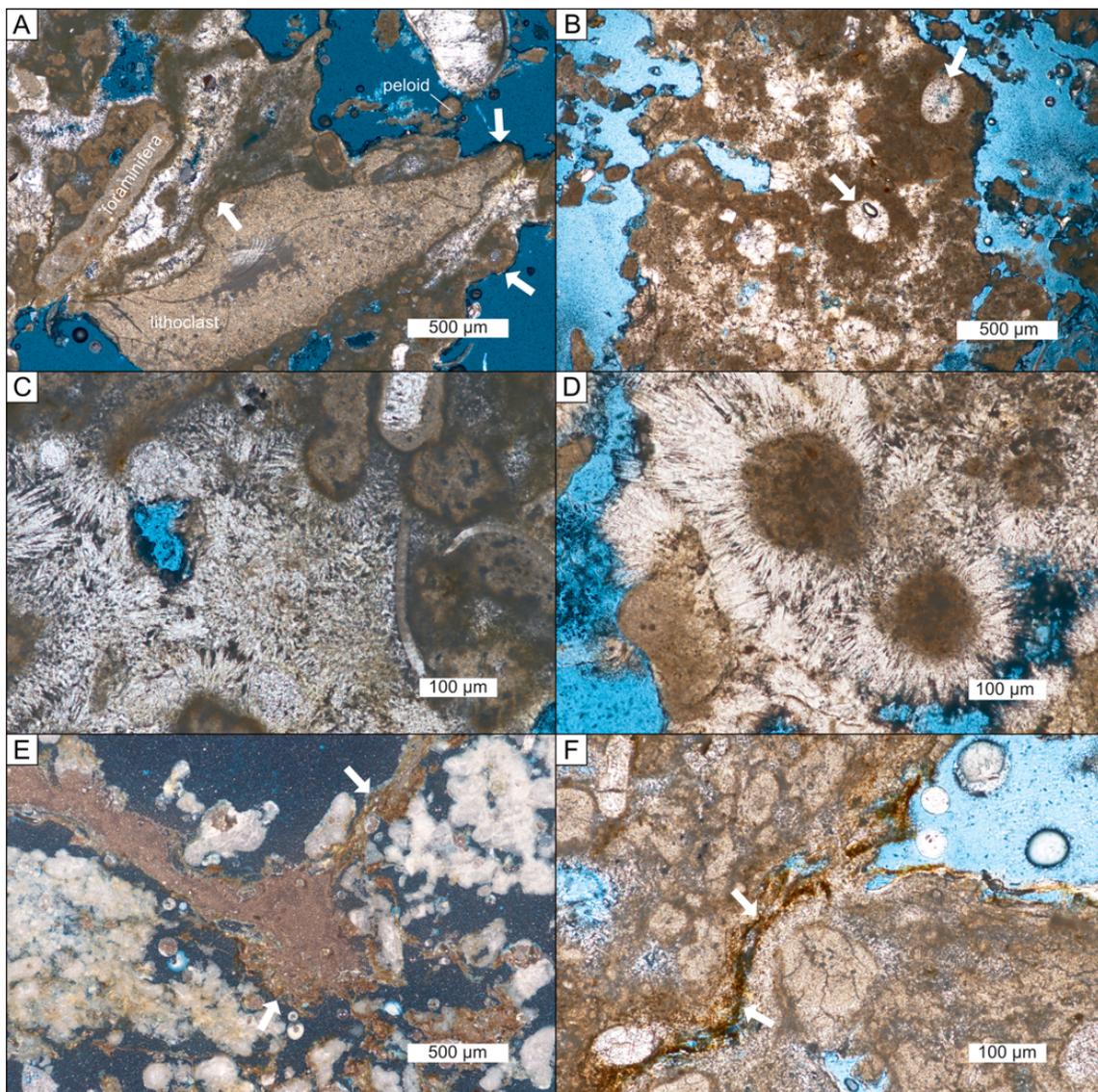
Figure 12: Thin section photomicrographs of stromatolites from the pool margin. A) Lithoclasts are shown surrounded by microbial organic-rich laminae (arrow). B) Moldic porosity after peloids filled by acicular aragonite cements (arrows). C, D) Acicular aragonite cements filling intragranular pore space. E, F) Dark organic seams indicate previous microbial growth (arrow).
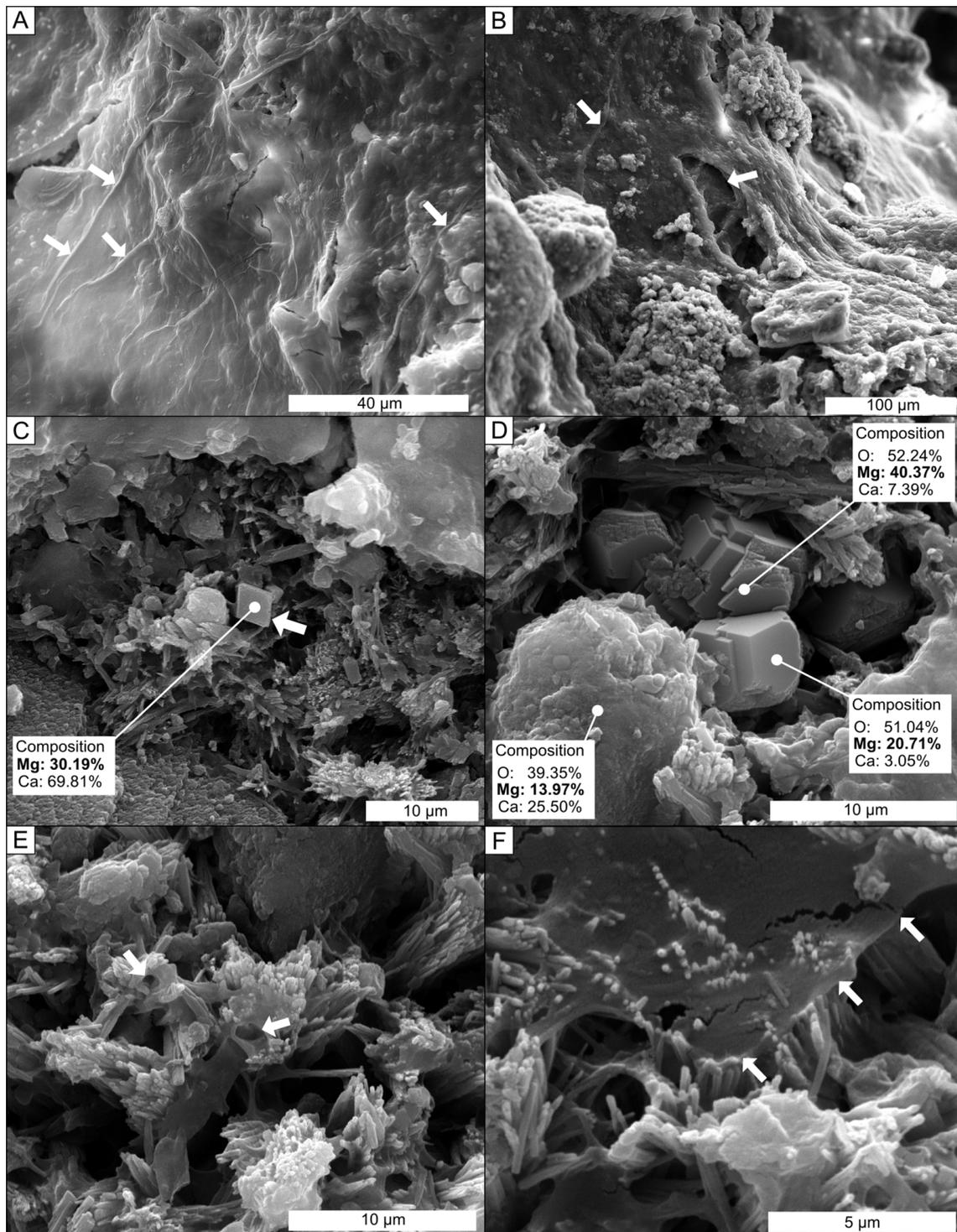
Figure 13: Scanning electron microscope micrographs. A, B) Extra-polymeric bacterial substance covering some areas of stromatolite specimen from the pool margin. Note bacterial filaments (white arrows). C) Crystal showing a very high Mg content indicative of proto-dolomite or true (arrow). The crystal is surrounded by aragonite cement and bacterial EPS. D) Another group of proto-dolomite crystals with very high Mg contents, surrounded by bacterial filaments, EPS and aragonite. E) Mineral precipitates in the stromatolites showing cyanobacterial tubes (arrows). F) Acicular aragonite covered by a layer of EPS (arrows).
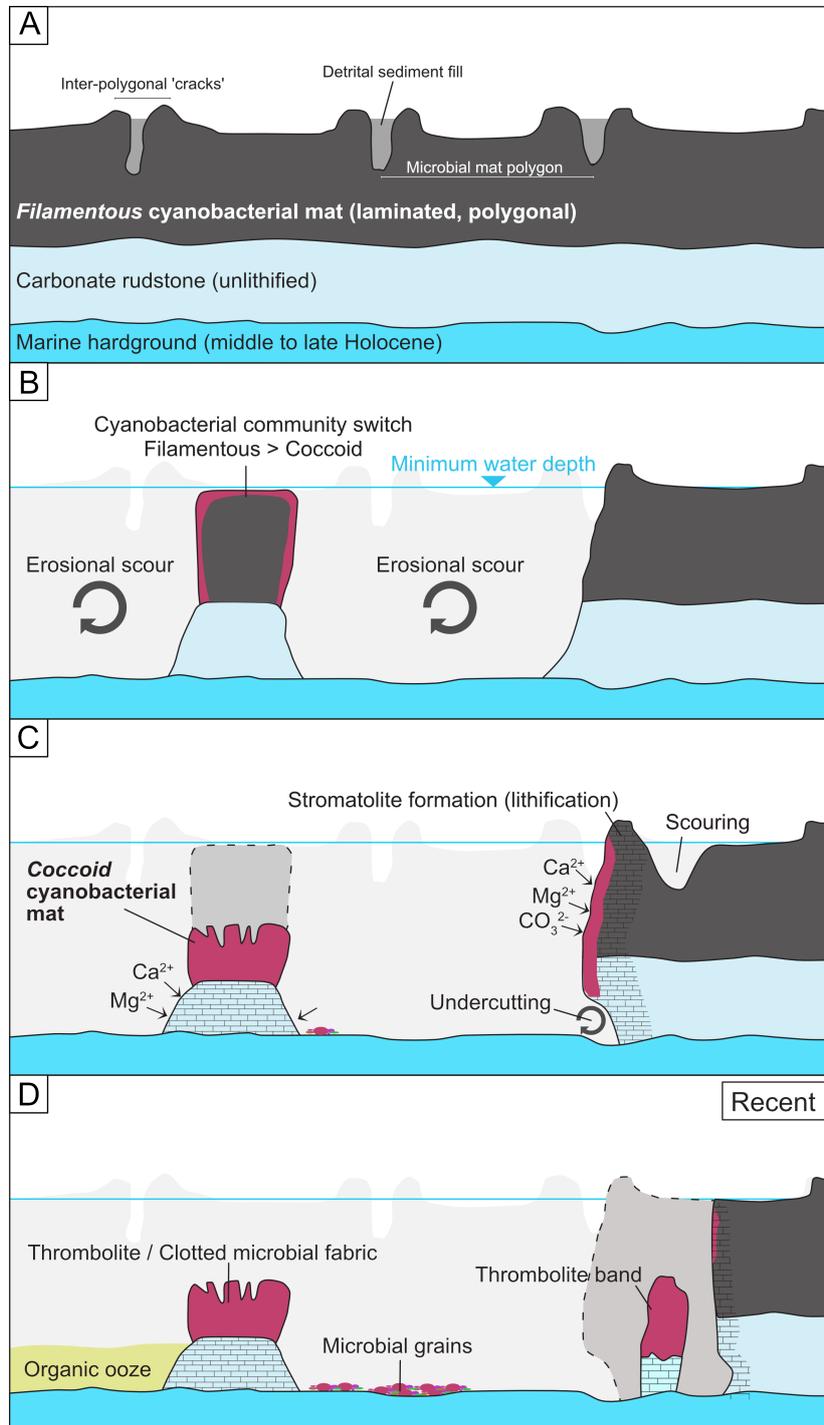
Figure 14: Schematic model of pool formation and lithification in the coastal sabkha of Abu Dhabi as explained in the text.
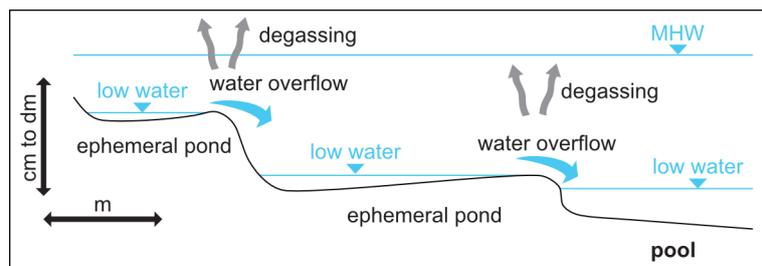
Figure 15: Schematic overview of the process that leads to permanent water coverage of the pool sensu travertine terraces. During high tide (MHW = mean high water) the pool and ephemeral pond system are fully covered by a maximum of 109 cm of water. During low tide the ephemeral ponds system slowly empties its excess water into the pool. Since this takes much longer than one 12 hour tidal cycle the pool is always filled with water. In addition, degassing occurs at areas at or near the water surface, leading to the precipitation of aragonite cements sensu the processes occurring at travertine terraces.